

Impact of Phase Noise and Oscillator Stability on Ultra-Narrow-Band-IoT Waveforms for Satellite

Christian A. Hofmann, Kai-Uwe Storek and Andreas Knopp
Bundeswehr University Munich, Chair of Signal Processing, 85579 Neubiberg, Germany.
Email: papers.sp@unibw.de

Abstract—It has been shown that ultra-narrow-band (uNB) massive machine type communication using very compact devices with direct access to satellites is possible at ultra low rate. This enables global ubiquitous coverage for terminals without terrestrial service in the Internet of Remote Things and provides access to any satellite up to the geostationary earth orbit. The lower data rate for waveforms providing uNB communication is set by the stability and the phase noise of the applied oscillators. In this paper we analyze the physical layer of two candidate waveforms, which are LoRa and Unipolar Coded Chirp-Spread Spectrum (UCSS) with respect to phase noise and oscillator frequency drifts. It is figured out that UCSS is more robust against linear frequency drifts, which is the main source of error for uNB transmissions.

I. INTRODUCTION

Narrow-band (NB) massive machine type communication (mMTC) will be an indispensable part of future mobile communication. For worldwide, seamless communication or continued service in remote areas, satellite systems enable global ubiquitous coverage in the Internet of Remote Things (IoRT) [1]. Satellite constellations in the low earth orbit (LEO) provide such coverage with a large number of satellites. They benefit from lower path loss and shorter latency compared to satellites at medium earth orbit (MEO) or geostationary earth orbit (GEO). The large number of required spacecraft for a worldwide, uninterrupted service leads to high costs for the system and subsequently high costs per transmitted bit for the subscribers. Satellite systems in GEO enabling machine type communication (MTC) in the Internet of Things (IoT) outside the polar regions with a small number of satellites usually operating at frequencies of the L-band or S-band. As these frequency bands do not offer much bandwidth, the costs for providing communication services are also quite high. At higher frequency bands like the C-Band or above, the link budget to GEO satellites offers only an ultra-narrow-band (uNB) communication with a few bits per second if very small transceivers are assumed and regulatory limits are met. Nevertheless, the large available bandwidths allow uNB communication for a vast number of devices at low cost. In [2] a novel uNB waveform called Unipolar Coded Chirp-Spread Spectrum (UCSS) has been presented that enables the random multiple access of very small devices to satellites in the GEO. The feasibility has been demonstrated at X-Band and Ku-Band frequencies [3]. The key to uNB communication is the efficient acquisition and synchronization of the signal that is received at very low power. Usually, the acquisition and

tracking performance of the applied algorithms sets the lower limit for the data rate. It is not simply possible to operate a waveform at a lower symbol rate to reduce the data rate and close the link budget. It has been shown in [3] that phase noise is limiting the correlation gain of spread spectrum waveforms and, hence, sets a lower limit for the symbol rate. In this paper we analyze the impact of phase noise on uNB communication in detail and demonstrate that the components of the phase noise with lower frequencies confine the symbol rate. We consider UCSS and LoRa, a chirp-spread spectrum (CSS) waveform, as candidates for uNB waveforms for satellite direct access.

In Section II, LoRa and UCSS are presented and the expected impact of phase noise on the waveforms is analyzed theoretically. Section III presents simulation results for the performance of the investigated waveforms under the impact of phase noise and linear frequency drifts. In Section IV, we provide measurement results that confirm the theoretical analysis and the simulation results. We conclude the paper in Section V.

II. CHIRP SPREAD SPECTRUM NARROWBAND WAVEFORMS

A. LoRa Basics

LoRa is a wireless communication technology that applies CSS for the modulation and enables communication at very low rate for terrestrial services [4], [5]. It is also considered for applications in LEO satellite systems [6]. LoRa uses a multiple frequency-shift keying (MFSK) modulation that is spread by linear chirps. An important parameter is the spreading factor S_F , which is usually given by $S_F = 2^{SF}$. Each symbol carries S_F bits and, hence, LoRa is a S_F -ary MFSK with S_F tones and chirp spreading.

For the transmission of N_{byte} bytes as payload, LoRa uses $N_S^{(\text{LoRa})}$ symbols if no payload header is added [7].

$$N_S^{(\text{LoRa})} = 8 + \max \left\{ \left\lceil \frac{8N_{\text{byte}}^{(\text{LoRa})} - 4 \cdot SF + 24}{4(SF - 2 \cdot \text{LDR})} \right\rceil (\text{CR} + 4), 0 \right\} \quad (1)$$

Here, $\text{CR} = 1, \dots, 4$ is used for the calculation of the coding rate $R_c = \frac{4}{4+\text{CR}}$, and LDR indicates the enabled low data rate optimization (LDRO). LDR = 1 stands for enabled, LDR = 0 for disabled. The LDRO parameter is usually set when the LoRa symbol time is equal or above 16.38 ms [8].

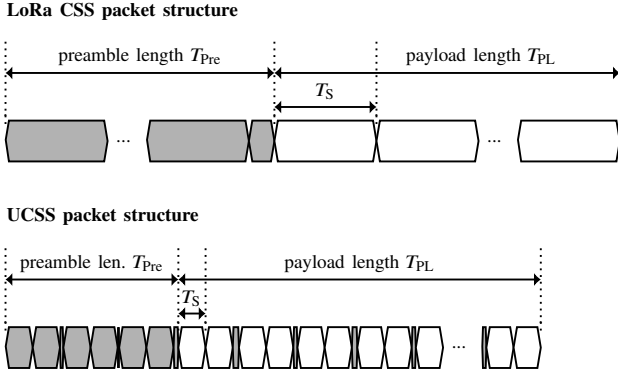


Fig. 1. LoRa and UCSS frame structure

The time T_S for the transmission of one chirp, i.e. one symbol, is given by $T_S = \frac{S_F}{R_s}$, where $R_s = 1/T_S$ stands for the sample rate.

Thus, all symbols of one frame are transmitted within the time $T_{PL}^{(LoRa)} = T_S \cdot N_S^{(LoRa)}$.

LoRa typically uses $N_{pre} = 12.25$ symbols for the preamble, which then covers a time $T_{pre}^{(LoRa)} = T_S \cdot N_{pre}^{(LoRa)}$. The structure of a transmitted LoRa frame is depicted in Fig. 1. Finally, the data rate in bit/s is given by

$$R_{bit}^{(LoRa)} = \frac{8 \cdot N_{byte}}{T_{pre}^{(LoRa)} + T_{PL}^{(LoRa)}} \quad (2)$$

and the transmission overhead $O^{(LoRa)}$ is

$$O^{(LoRa)} = 1 - \frac{T_{PL}^{(LoRa)}}{T_{fr}^{(LoRa)}}. \quad (3)$$

Table I lists the calculated parameters for different settings of R_s and SF, which are also used in this paper for simulations and measurements.

B. Impact of Phase Noise on LoRa

It has been shown that the requirements on the phase noise performance of oscillators are quite relaxed when frequency-shift keying (FSK) modulation is used [9]. As also shown by simulation in subsection III-A, the faster phase noise components (i.e. the white frequency-, flicker phase-, and white phase noise component) are not harmful to LoRa modulation. On the other hand, random frequency walk and flicker frequency noise are affecting its performance. For LoRa, the frequency drift of the local oscillator (LO) is one of the most relevant parameters limiting the maximum packet length [10]. This becomes obvious if the carrier frequency offset (CFO) between transmitter (Tx) and receiver (Rx) is considered. If we assume that the CFO is estimated and compensated perfectly only at the beginning of a packet, then a symbol error occurs whenever a tone out of the MFSK alphabet is shifted towards the neighboring tone beyond the decision boundary. With LoRa, the distance in frequency between any two tones is given by [8]

$$\Delta f_S = \frac{R_s}{S_F}. \quad (4)$$

This means that a symbol error occurs if the CFO is larger than $0.5 \cdot \Delta f_S$. This leads to the limit for the maximum frequency offset $\Delta f_{max}^{(LoRa)}$ that may occur during the timespan of one frame

$$\Delta f_{max}^{(LoRa)} = \frac{R_s}{3 \cdot 2^{SF}}, \quad (5)$$

provided in the LoRa documentation [8].

For higher values of SF and lower values of R_s , the neighboring symbols have a quite small distance Δf_S , and the modulation is very sensitive to drifting CFO. Therefore, the LDRO parameter is set (LDR = 1) if $T_S \geq 16.38$ ms. In that case, the number of bits per symbol is reduced by two and the maximal frequency shift during a single packet transmission provided in [8] is relaxed to $\Delta f_{max}^{(LoRa,LDR)}$ given by

$$\Delta f_{max}^{(LoRa,LDR)} = 16 \cdot \Delta f_{max}^{(LoRa)}. \quad (6)$$

This value given by the data sheet is larger than the frequency difference between neighboring tones with LDR = 1 given by

$$\Delta f_S = \frac{R_s}{2^{SF-2}}. \quad (7)$$

This means that practical LoRa receivers somehow track the CFO to improve the resistance against frequency drift. If we assume a linear drift of the CFO with rate \mathcal{D} , then the maximum drift rate \mathcal{D}_{max} defining the upper limit for the successful transmission of a frame is calculated from the length of the payload T_{PL} by¹

$$\mathcal{D}_{max} = \frac{\Delta f_{max}}{T_{PL}}. \quad (8)$$

For LoRa devices an analysis on CFO drift of practical devices is published in [10], where an almost linear frequency drift over time is observed, while the circuit is heated by the radio frequency (RF) components in burst transmission. Drift rates $\mathcal{D} = \frac{\delta f(t)}{\delta t}$ between 20 Hz/s and 80 Hz/s are reported for a Semtech reference design PCB at 915 MHz, at 25°C in a +15 dBm transmit operation. The drift is reduced to values between 10 Hz/s and 30 Hz/s by thermal isolation of the oscillator and to <20 Hz/s if a temperature compensated crystal oscillator (TCXO) is used.

In [11] LoRa has been analyzed with respect to dynamic Doppler shifts and limits for maximum frequency drifts are determined by measurements. The authors delivered, the maximum allowable frequency drift of 4.94 ppm/s and 0.33 ppm/s at 434 MHz with symbol rates of 250 kHz and 125 kHz for SF 11 and 12, respectively. These values are higher than the specified values in [8] and couldn't be confirmed by our measurements.

From Table I it is derived that the drift rates provided in [10] are too high to guarantee a successful transmission with all settings for R_s and SF.

A countermeasure for a transmission at the given drift rates \mathcal{D} at lower symbol rate is to shorten the frame length. By this, T_{PL} becomes shorter and \mathcal{D}_{max} is increased. Unfortunately,

¹Here, we assume that the CFO is compensated perfectly at the end of the preamble.

the LoRa transmission is very inefficient at very short frame lengths, because the fixed preamble length of the standard produces a significant amount of overhead. Therefore, we consider UCSS in the following, which has been developed with respect to efficient transmission with short frames.

C. UCSS Basics

UCSS promises efficient communication with reduced overhead at very low rates [12]. The main idea is to introduce short pause times between the chirps to separate and identify users transmitting simultaneously, while the phase of the chirps is modulated to carry information. With UCSS it is possible to transmit at ultra-low rate and provide access to satellites in GEO for very small devices at higher frequencies, where sufficient spectrum is available for mMTC.

For UCSS, only a short header with pilot symbols for CFO estimation is required as depicted in Fig. 1. Further overhead is caused by the pause times between the symbols, which become longer, the more symbols are transmitted within one packet. Hence UCSS is suitable for efficient transmission of short blocks at ultra-low signal to noise power ratios (SNRs).

We provide settings for the spreading factor S_F and the symbol rate R_s of UCSS that require similar sensitivity like the settings for LoRa. Equal setting numerals in Table I for both waveforms indicate similar required SNR for successful transmission. Here, the waveforms are compared by their frame-error rate (FER) over the SNR measured by simulations in additive white Gaussian noise (AWGN) without further errors or synchronization. The values for the required SNR in Table I are found in [8].

Fairness is ensured as the waveforms are compared when operating in the same bandwidth with the same transmit power. Although UCSS is a waveform enabling random multiple access, we consider only one active user here, for the sake of a fair comparison.

The number of symbols N_S within a UCSS frame is calculated by

$$N_S^{(\text{UCSS})} = \frac{N_{\text{byte}} \cdot 8 + N_{\text{CRC}}}{R_c} \quad (9)$$

where $N_{\text{CRC}} = 3$ is the number of bits used for a cyclic redundancy check (CRC). Here, we use a header with $N_{\text{pre}} = 6$ symbols for CFO estimation. The length T_{pause} of the pause times between the symbols depends on the used unipolar code [12] and is given by

$$T_{\text{pause}} = \left\lceil \frac{N_S^{(\text{UCSS})}}{2} \right\rceil^2 / R_s. \quad (10)$$

Thus, the duration of the entire frame is given by

$$T_{\text{fr}}^{(\text{UCSS})} = T_{\text{pre}}^{(\text{UCSS})} + T_{\text{PL}}^{(\text{UCSS})} + T_{\text{pause}}, \quad (11)$$

and the transmission overhead $O^{(\text{UCSS})}$ is

$$O^{(\text{UCSS})} = 1 - \frac{T_{\text{PL}}^{(\text{UCSS})}}{T_{\text{fr}}^{(\text{UCSS})}}. \quad (12)$$

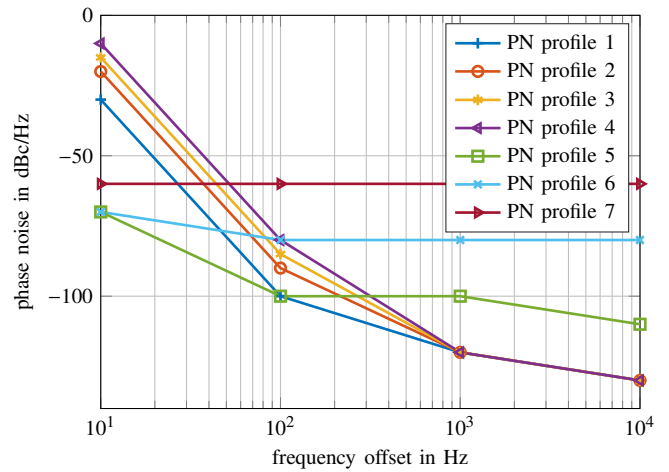


Fig. 2. Phase noise power spectral density (PSD) profiles used for simulation of phase noise

D. Impact of Phase Noise on UCSS

As UCSS is a differentially modulated waveform, a symbol error due to a CFO is very unlikely. In fact, a false decision for a symbol occurs if the CFO shifts the phase during the time between two differential binary phase-shift keying (DBPSK) symbols by more than $\pi/4$. The resulting values $\Delta f_{\text{max}}^{(\text{UCSS})}$ for the CFO causing a symbol error are quite high. Instead, the maximum CFO is limited for UCSS by the timeshift of the chirp symbols. As any frequency shift of a chirp is linked to a shift of the chirp in time domain, the chirp is shifted by the CFO in time and no longer detected if the CFO is too high. Thus, the maximum CFO is not given by $\Delta f_{\text{max}}^{(\text{UCSS})}$ but is instead approximately calculated by

$$\Delta f_{\text{max}}^{(\text{UCSS})} \approx \frac{1}{2} \cdot \frac{R_s}{S_F}. \quad (13)$$

This is further analyzed by simulation in Section III-B.

III. SIMULATION RESULTS

A. Phase Noise

In this subsection we analyze the impact of phase noise on the performance of LoRa and UCSS. First, we demonstrate that both CSS waveforms perform well under the influence of fast phase noise (white frequency-, flicker phase-, and white phase noise), while slow phase noise (random frequency walk and flicker frequency) is harmful to UCSS and LoRa. Therefore, we use different phase noise power spectral density (PSD) profiles as depicted in Fig. 2. Starting at the realistic profile 1, we increase only the slow phase noise from profile 1 to profile 4. From profile 5 to profile 7, the fast phase noise is increased incrementally.

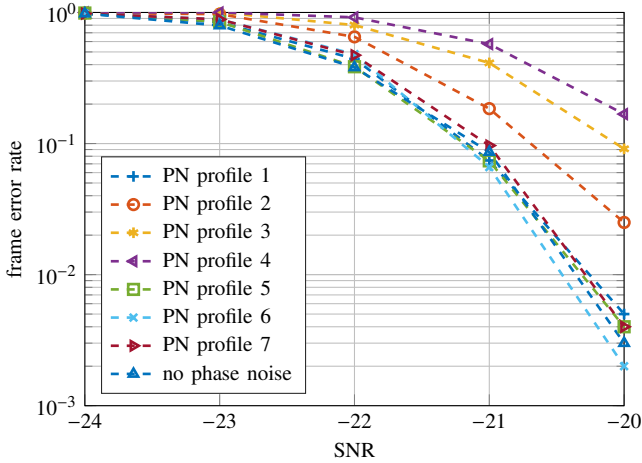
The simulation is performed in MATLAB using the phase noise system object, which applies a filtered, white noise signal for the phase error. The filter coefficients are calculated from the profiles of Fig. 2 according to [13].

For the simulation of LoRa we applied the code from [5] and further implemented the LDRO. The simulations

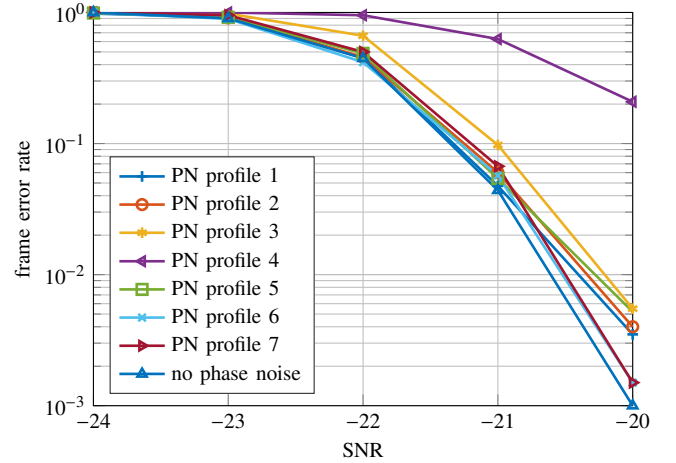
TABLE I
 SETTINGS AND PARAMETERS FOR LoRa AND UCSS. EQUAL SETTING NUMERALS FOR BOTH WAVEFORMS INDICATE SIMILAR REQUIRED SNR FOR SUCCESSFUL TRANSMISSION

| Parameter | Symbol | Unit | LoRa | | | | | |
|----------------------|----------------------------|-------|-------|-------|-------|-------|-------|-------|
| | | | LS-1 | LS-2 | LS-3 | LS-4 | LS-5 | LS-6 |
| Setting Nr. | | | | | | | | |
| Sample Rate | R_s | kHz | 62 | 20 | 20 | 20 | 20 | 20 |
| Spreading | SF | | 9 | 9 | 10 | 11 | 12 | 12 |
| Code Rate | CR | | 0,5 | 0,5 | 0,5 | 0,5 | 0,5 | 1,0 |
| LDR on | LDR | | 0 | 1 | 1 | 1 | 1 | 1 |
| User Bytes | N_{byte} | bytes | 16 | 8 | 8 | 8 | 8 | 4 |
| Symbols | N_S | | 40 | 24 | 24 | 24 | 16 | 12 |
| Sym. Duration | T_S | ms | 8,3 | 25,6 | 51,2 | 102,4 | 204,8 | 204,8 |
| Payl. Duration | T_{PL} | ms | 330 | 614 | 1229 | 2458 | 3277 | 2458 |
| Preamble Sym. | N_{Pre} | | 12,25 | 12,25 | 12,25 | 12,25 | 12,25 | 12,25 |
| Prea. Duration | T_{Pre} | ms | 101 | 314 | 627 | 1254 | 2509 | 2509 |
| Packet Dur. | T_{Fr} | ms | 431 | 928 | 1856 | 3712 | 5786 | 4966 |
| Required SNR | Γ_{min} | dB | -12,5 | -12,5 | -15,0 | -17,5 | -20,0 | -20,0 |
| Data Rate | R_{bit} | bit/s | 296,7 | 69,0 | 34,5 | 17,2 | 11,1 | 6,4 |
| Overhead | $O(\text{LoRa})$ | | 23% | 34% | 34% | 34% | 43% | 51% |
| Max. CFO Datasheet | Δf_{max} | Hz | 40,4 | 208,3 | 104,2 | 52,1 | 26,0 | 26,0 |
| Max. Drift Datasheet | \mathcal{D}_{max} | Hz/s | 93,5 | 224,5 | 56,1 | 14,0 | 4,5 | 5,2 |

| Parameter | Symbol | Unit | UCSS | | | | | |
|----------------|----------------------------|-------|-------|-------|-------|-------|-------|-------|
| | | | US-1 | US-2 | US-3 | US-4 | US-5 | US-6 |
| Setting Nr. | | | | | | | | |
| Sample Rate | R_s | kHz | 62 | 20 | 20 | 20 | 20 | 20 |
| Spreading | S_F | | 67 | 67 | 117 | 211 | 373 | 373 |
| Code Rate | R_c | | 0,5 | 0,5 | 0,5 | 0,5 | 0,5 | 0,5 |
| PauseTimes | | ms | 72 | 224 | 224 | 224 | 224 | 61 |
| User Bytes | N_{byte} | bytes | 8 | 8 | 8 | 8 | 8 | 4 |
| Symbols | N_S | | 134 | 134 | 134 | 134 | 134 | 70 |
| Sym. Duration | T_S | ms | 1,1 | 3,4 | 5,9 | 10,6 | 18,7 | 18,7 |
| Payl. Duration | T_{PL} | ms | 145 | 449 | 784 | 1414 | 2499 | 1306 |
| Preamble Sym. | N_{Pre} | | 6 | 6 | 6 | 6 | 6 | 6 |
| Prea. Duration | T_{Pre} | ms | 6 | 20 | 35 | 63 | 112 | 112 |
| Packet Dur. | T_{Fr} | ms | 224 | 693 | 1043 | 1701 | 2835 | 1479 |
| Required SNR | Γ_{min} | dB | -12,6 | -12,6 | -15,0 | -17,5 | -20,0 | -20,0 |
| Data Rate | R_{bit} | bit/s | 286,1 | 92,3 | 61,3 | 37,6 | 22,6 | 21,6 |
| Overhead | $O(\text{UCSS})$ | | 35% | 35% | 25% | 17% | 11,9% | 11,7% |
| Max. CFO (13) | Δf_{max} | Hz | 463 | 149 | 85 | 47 | 27 | 27 |
| Max. Drift | \mathcal{D}_{max} | Hz/s | 3195 | 332 | 109 | 34 | 11 | 21 |



(a) LoRa frame error rate; $R_s = 20$ kHz, SF = 11 (setting LS-4)



(b) UCSS frame error rate; $R_s = 20$ kHz, $S_F = 211$ (setting US-4).

Fig. 3. Frame error rate over the SNR for different phase noise PSD profiles as given in Fig. 2

were performed in AWGN without introducing further errors (frequency, clock) and further synchronization algorithms at the receiver. The results for the FER over the SNR are shown in Fig. 3a. The figure reveals that only profiles 2, 3 and 4 are negatively affecting the performance of LoRa, indicated by an increased FER.

We repeated the simulation using UCSS with the parameters provided in the caption of Fig. 3b. The presented results there also indicate, that only the slow phase noise degrades the performance of UCSS. In comparison to LoRa, it can be observed that LoRa is slightly stronger affected by slow phase noise components.

We focus on slow phase noise in the remainder of this paper as this is the most harmful distortion for UCSS and LoRa. We

consider the linear frequency drift as a kind of worst case and, thus, we determine the maximum CFO drift rate for both waveforms.

B. Linear Frequency Drift

In the following, we present simulation results for LoRa and UCSS under the influence of a linearly increasing CFO. Here, the N_{rx} receive signal samples $r[n]$ with $n = 0, \dots, N_{\text{rx}} - 1$ are calculated from the transmit signal samples $x[n]$ by

$$r[n] = x[n] \cdot \phi \cdot \Phi[n] + \eta[n] \quad (14)$$

where ϕ is a random phase in $[0, 2\pi[$ and $\eta[n]$ stands for complex Gaussian noise with variance σ_η^2 so that the desired

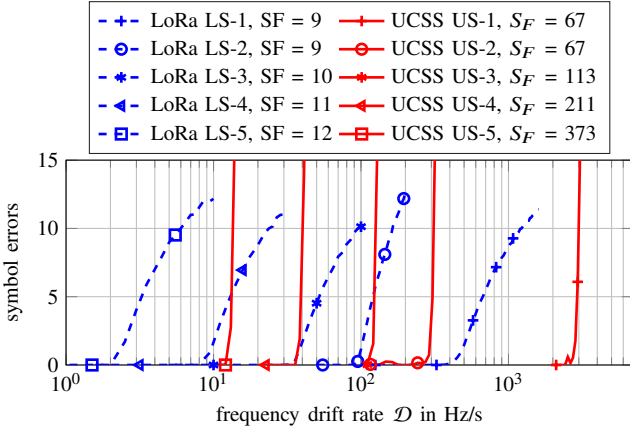


Fig. 4. Number of symbol errors for LoRa and UCSS versus the the frequency drift rate. Marker symbols indicate the same requirement on the SNR.

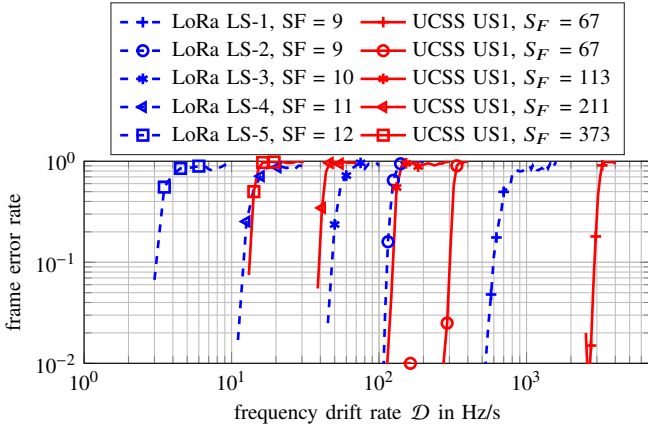


Fig. 5. Simulation results for the frame error rate (FER) of LoRa and UCSS versus the the frequency drift rate. Marker symbols indicate the same requirement on the SNR.

SNR $\Gamma = \frac{\sigma_x^2}{\sigma_n^2}$ is achieved. The CFO drift $\Phi[n]$ is

$$\Phi[n] = \exp \left\{ j 2\pi \left(n \frac{\mathcal{D} \cdot T_{\text{PL}}}{N_{\text{rx}}} \right) n T_s \right\} \quad (15)$$

to ensure that the CFO Δf after T_{PL} is $\Delta f = \mathcal{D} \cdot T_{\text{PL}}$.

The Monte Carlo simulations in AWGN are performed at an SNR ensuring a 3 dB margin from the required SNR provided in Table I. When regarding Fig. 4, it is observed that the number of symbol errors is increasing over the increasing frequency drift rate \mathcal{D} . In the figure, the blue dashed curves stand for LoRa and the red solid curves for UCSS. The same marker symbols indicate comparable settings for both modulations with the same requirement on the SNR. The figure reveals that UCSS is more robust against drifting CFO than LoRa for all settings analyzed here. This is also derived from Fig. 5 where the FER is plotted over the frequency drift rate.

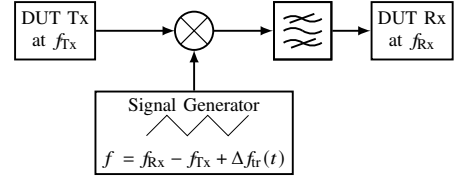


Fig. 6. Measurement Setup

IV. MEASUREMENT RESULTS

To verify the simulation results in practice, we performed measurements with LoRa hardware and a software defined radio (SDR) implementation of UCSS. We used two Semtech SX1261/SX1262 Development Kits as LoRa Tx and Rx. For UCSS, an SDR Ettus USRP B205 was used as Tx and a B210 as Rx. The devices were connected in a test setup according to Fig. 6, where the Tx was operated at center frequency f_{Tx} while the receiver was receiving at f_{Rx} . A frequency conversion with a time variant LO $\Delta f_{\text{tr}}(t)$ introduced a linear frequency drift. Here, $\Delta f_{\text{tr}}(t)$ was a triangle wave with

$$\Delta f_{\text{tr}}(t) = 2 \cdot \Delta f_{\text{max, tr}} \left| \frac{t}{T_{\text{tr}}} - \left\lfloor \frac{t}{T_{\text{tr}}} + \frac{1}{2} \right\rfloor \right|, \quad (16)$$

where T_{tr} is the period of the triangle wave given by

$$T_{\text{tr}} = \frac{\Delta f_{\text{max, tr}}}{\mathcal{D}^{(\text{meas})}} \quad (17)$$

to ensure a linear frequency drift with rate $\mathcal{D}^{(\text{meas})}$. The maximum CFO $\Delta f_{\text{max, tr}}$ was chosen such that the receivers were still able to operate at $\Delta f_{\text{max, tr}}$ without performance degradation. We used $\Delta f_{\text{max, tr}} = \frac{1}{4} R_s$ in our tests. During the measurements we used $f_{\text{Tx}} = 830 \text{ MHz}$ and $f_{\text{Rx}} = 880 \text{ MHz}$ for both waveforms.

Fig. 7 depicts the measured FER for LoRa and UCSS over the frequency drift rate $\mathcal{D}^{(\text{meas})}$. The measurement results confirm the simulation very well. For LoRa it is observed that the robustness against CFO drift predicted by the datasheet is confirmed in practice for higher data rates. At the ultra low rate given by setting LS-5, the datasheet predicts a maximum rate of 4.5 Hz/s, while only 2 Hz/s were tolerable in the measurements. The setting with the lowest data rate for UCSS (US-5) was able to withstand a CFO drift of up to 10 Hz/s in our measurements. This is approximately 5 Hz/s less than observed from the simulation results. Of course the frequency drift of the oscillators of Tx and Rx hardware during the measurements cannot be ignored and is added to the drift introduced by the LO. Although we kept the Tx and Rx in an environment with constant temperature and operated them in continuous mode to avoid heating of the LO in burst mode, the residual drift obviously affected the measured results. Nevertheless, the measurement results are very close to the simulation results and finally confirm our theoretical assumptions.

Both waveforms can be adopted to withstand CFO drifts with even higher rates than presented here if they occur in practice. This is achieved by shorter frames with less bytes

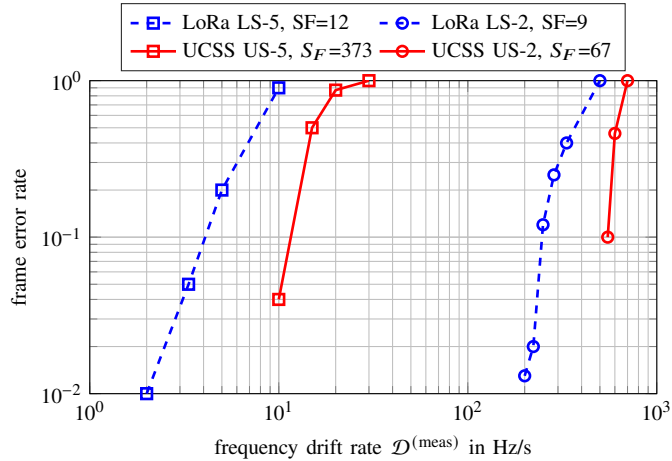


Fig. 7. Measured frame error rate (FER) for LoRa and UCSS at $f_x = 830$ MHz and $f_{Rx} = 880$ MHz with $R_s = 20$ kHz

within the payload. Another countermeasure to CFO drifts would be the insertion of pilot symbols within the frame, which of course also increases the overhead. The relationship between payload length and robustness against CFO drift is shown in Table I by the comparison of the settings 5 and 6. The drawback for LoRa is the increased overhead if the payload is shortened. This is derived from Table I where the communication overhead for LoRa is increasing from 43% to 51% for 8 bytes and 4 bytes per frame in setting LS-5 and LS-6, respectively. On the other hand, the overhead of UCSS is slightly reduced if shorter frames are used in settings US-5 and US-6. Hence, UCSS not only shows a better robustness against CFO drifts than LoRa but also is able to transmit with less overhead.

V. CONCLUSION

In this paper we analyzed the impact of phase noise and frequency drift on two candidate waveforms for satellite ultra-narrow-band transmission. With LoRa and UCSS, we considered and compared two CSS waveforms by simulation and measurements in the laboratory. Both waveforms are not sensitive to fast phase noise components, while the slower components of the phase noise (random frequency walk and flicker frequency noise) are affecting the transmissions. We concentrated our analysis to the most harmful phase error, which is a linear frequency drift. We derived the maximum tolerable drift rate for the successful transmission of a frame at different sample rates and spreading factors. UCSS showed an increased robustness against drifting carrier frequencies in all investigated settings compared to the equivalent LoRa setting. Furthermore, UCSS allows the shortening of the transmitted frames without increasing the transmission overhead and, thus, is able to increase the robustness against linear frequency drifts if necessary.

REFERENCES

- [1] M. De Sanctis, E. Cianca, G. Araniti, I. Bisio, and R. Prasad, "Satellite communications supporting internet of remote things," *IEEE Internet Things J.*, vol. 3, no. 1, pp. 113–123, feb 2016.
- [2] C. A. Hofmann and A. Knopp, "Ultra-Narrowband Waveform for IoT Direct Random Multiple Access to GEO Satellites," *IEEE Internet Things J.*, vol. 6, no. 6, pp. 10 134–10 149, dec 2019.
- [3] —, "Direct Access to GEO Satellites: An Internet of Remote Things Technology," in *2019 IEEE 2nd 5G World Forum - WS7 - Work. Satell. Non-Terrestrial Networks 5G*. Dresden: IEEE, sep 2019, pp. 1–6.
- [4] U. Raza, P. Kulkarni, and M. Sooriyabandara, "Low power wide area networks: A survey," *IEEE Commun. Surv. Tutorials*, vol. 19, no. 2, 2017.
- [5] H. Mroue, A. Nasser, B. Parrein, S. Hamrioui, E. Mona-Cruz, and G. Rouyer, "Analytical and Simulation study for LoRa Modulation," in *2018 25th Int. Conf. Telecommun. ICT 2018*. IEEE, jun 2018, pp. 655–659.
- [6] Lacuna, "Lacuna Space achieves major milestone for LoRa® in Space – Lacuna," 2020.
- [7] Semtech Corporation, "SX1272/3/6/7/8 LoRa Modem Design Guide, AN1200.13," no. July, p. 9, 2013.
- [8] Semtech, "SX1261/2 Long Range, Low Power, sub-GHz RF Transceiver, DS.SX1261-2.W.APP," Tech. Rep., 2017.
- [9] X. Chen, H. S. Kim, and D. D. Wentzloff, "An analysis of phase noise requirements for ultra-low-power FSK radios," in *Dig. Pap. - IEEE Radio Freq. Integr. Circuits Symp.* IEEE, jun 2017, pp. 37–40.
- [10] Semtech Corporation, "Application Note: Recommendations for Best Performance, AN1200.37," p. 16, 2018.
- [11] A. A. Doroshkin, A. M. Zadorozhny, O. N. Kus, V. Y. Prokopyev, and Y. M. Prokopyev, "Experimental Study of LoRa Modulation Immunity to Doppler Effect in CubeSat Radio Communications," *IEEE Access*, vol. 7, pp. 75 721–75 731, 2019.
- [12] C. A. Hofmann and A. Knopp, "Ultrawideband Waveform for IoT Direct Random Multiple Access to GEO Satellites," *IEEE Internet Things J.*, vol. 6, no. 6, pp. 10 134–10 149, dec 2019.
- [13] N. J. Kasdin, "Discrete Simulation of Colored Noise and Stochastic Processes and $1/f^\alpha$ Power Law Noise Generation," *Proc. IEEE*, vol. 83, no. 5, pp. 802–827, may 1995.